

KOITER'S POST-BUCKLING ANALYSIS OF GENERAL SHELL STRUCTURES USING THE FINITE ELEMENT METHOD

P. Tiso, M.M.Abdalla , E.L. Jansen
Delft University of Technology, Delft, The Netherlands

Keywords: *Post-buckling, Perturbation, Finite Elements, Shells*

Abstract

We present in this paper a simple finite element implementation of Koiter's perturbation analysis for initial post-buckling of general shell structures. The calculation of post-buckling curvature coefficients shows converge problems when careless finite element implementation of Koiter's analysis is carried out. Instead of using special formulations, we show that reasonably accurate results can be obtained by extending an existing linear triangular shell element with a nonlinear strain contribution derived from simple linear displacement shape functions. The resulting constant strains alleviate locking phenomena in the calculation of the post-buckling coefficients. Numerical results are shown to validate the proposed approach.

1 Introduction

Thin-walled structures constitute main structural components for, among other fields, aerospace constructions. Their favorable strength-to-weight ratio together with their slenderness often makes the buckling strength the key design criterion. Moreover, some structural configurations lead to sensitivity of the response to geometrical or load imperfections. The structure is said to be "imperfection-sensitive" and the post-buckling behavior exhibits an unstable path. This can result in a relevant reduction of the maximum load carrying capacity for the imperfect structure with respect to the "perfect" one. Another aspect should be considered. An optimized de-

sign often leads to clustering of buckling loads and results in the interaction between different buckling modes in the post-buckling path. This can render the structure extremely imperfection sensitive, and often local and global modes interact. The numerical prediction of the nonlinear response of a general thin-walled structure often relies on non-linear finite element analysis. Complex post-buckling paths can be tracked by the use of path-following techniques [12]. These methodologies are quite computationally expensive and not practical in a design stage when several analyzes are required. In presence of mode interactions, path-following methods require sometimes special tuning to handle such situations. Asymptotic methods such the one proposed by Koiter [2] stand as a competitive tool for the prediction of the post-buckling behavior of thin-walled structures. The solution is expanded in a power series around a bifurcation point and the load-deflection path is reconstructed via a series of expansion coefficients that are a "property" of the perfect structure, i.e. are calculated once for all for a given structure. Then, the contribution of the imperfection can just be added a posteriori with negligible additional computational cost. Koiter's method has been recently implemented in a finite element framework, for instance [11, 10, 4, 6, 9, 8]. In particular, numerical problems associated to the numerical implementation and poor convergence of the post-buckling coefficients have been addressed. In all the referenced works, the use of special finite element formulations and ad-hoc enrichment techniques has been proposed to overcome these is-

sues. We will show here that it is possible to obtain accurate results by applying Koiter's method using a general well established shell element without any cumbersome addition or reformulation.

2 Asymptotic post-buckling analysis

We use in this section the notation introduced by Budiansky et al. in [3]. This notation is extremely compact and could be applied to either continuous or discrete problems. The equivalent finite element notation is presented in the next section. We denote with \mathbf{u} , $\boldsymbol{\varepsilon}$, and $\boldsymbol{\sigma}$ a generalized displacement, strain and stress field respectively. Each symbol can be thought as a vectorial entity, its specific dimension depending on the particular problem at hand. The strain-displacement relation is assumed quadratic, as

$$\boldsymbol{\varepsilon} = L_1(\mathbf{u}) + \frac{1}{2}L_2(\mathbf{u}) \quad (1)$$

where L_1 and L_2 are linear and quadratic functional respectively. The stress-strain relation is

$$\boldsymbol{\sigma} = H(\boldsymbol{\varepsilon}) \quad (2)$$

where H is a linear functional. The structure is loaded by a load distribution \mathbf{q} and the static equilibrium is governed by the principle of virtual works

$$\boldsymbol{\sigma} \cdot \delta\boldsymbol{\varepsilon} = \mathbf{q} \cdot \delta\mathbf{u}. \quad (3)$$

In equation 3 the "dot" operation is a shorthand notation that, in term $\mathbf{a} \cdot \mathbf{b}$, means the virtual work of stresses (or loads) \mathbf{a} through the strains (or displacements) \mathbf{b} , integrated over the whole structure. Equation 3 must hold for all possible admissible variations $\delta\mathbf{u}$ for the equilibrium of the structure, i.e. variations consistent with the kinematic boundary conditions. Here $\delta\boldsymbol{\varepsilon}$ is the first order strain variation generated by $\delta\mathbf{u}$. If a bilinear functional operator L_{11} is defined as

$$L_2(\mathbf{u} + \mathbf{v}) = L_2(\mathbf{u}) + L_{11}(\mathbf{u}, \mathbf{v}) + L_2(\mathbf{v})$$

then the variation $\delta\boldsymbol{\varepsilon}$ resulting from $\delta\mathbf{u}$ is written as

$$\delta\boldsymbol{\varepsilon} = \delta\mathbf{e} + L_{11}(\mathbf{u}, \delta\mathbf{u}) \quad (4)$$

where $\mathbf{e} \equiv L_1(\mathbf{u})$. Note that $L_{11}(\mathbf{u}, \mathbf{v}) = L_{11}(\mathbf{v}, \mathbf{u})$ and $L_{11}(\mathbf{u}, \mathbf{u}) = L_2(\mathbf{u})$.

It is further assumed that the reciprocal relation

$$H(\boldsymbol{\varepsilon}_1) \cdot \boldsymbol{\varepsilon}_2 = H(\boldsymbol{\varepsilon}_2) \cdot \boldsymbol{\varepsilon}_1 \quad (5)$$

holds for all $\boldsymbol{\varepsilon}_1$ and $\boldsymbol{\varepsilon}_2$. We consider in this study loads proportional to a parameter λ , i.e. $\mathbf{q} = \lambda\mathbf{q}_0$. The load pattern \mathbf{q} does not depend on the displacement \mathbf{u} .

The displacement, stress and strain fields that the structure attains in the pre-buckling path after the application of the static pre-load $\mathbf{q} = \lambda\mathbf{q}_0$ is considered linear, namely:

$$\begin{Bmatrix} \mathbf{u} \\ \boldsymbol{\varepsilon} \\ \boldsymbol{\sigma} \end{Bmatrix} = \lambda \begin{Bmatrix} \mathbf{u}_0 \\ \boldsymbol{\varepsilon}_0 \\ \boldsymbol{\sigma}_0 \end{Bmatrix} \quad (6)$$

The linearity of the pre-buckling field requires that

$$L_{11}(\mathbf{u}_0, \mathbf{v}) = 0 \quad (7)$$

for all \mathbf{v} . We have thus $\boldsymbol{\varepsilon}_0 = L_1(\mathbf{u}_0) = \mathbf{e}_0$ and $\boldsymbol{\sigma}_0 = H(\boldsymbol{\varepsilon}_0)$. The linear equilibrium is therefore governed by

$$\boldsymbol{\sigma}_0 \cdot \delta\mathbf{e} = \mathbf{q}_0 \cdot \delta\mathbf{u}. \quad (8)$$

To investigate the instability of the pre-buckling path, the solution is perturbed as follows:

$$\begin{Bmatrix} \mathbf{u} \\ \boldsymbol{\varepsilon} \\ \boldsymbol{\sigma} \end{Bmatrix} = \lambda \begin{Bmatrix} \mathbf{u}_0 \\ \boldsymbol{\varepsilon}_0 \\ \boldsymbol{\sigma}_0 \end{Bmatrix} + \xi_i \begin{Bmatrix} \mathbf{u}_i \\ \boldsymbol{\varepsilon}_i \\ \boldsymbol{\sigma}_i \end{Bmatrix} \quad (9)$$

in which

$$\boldsymbol{\varepsilon}_i = \mathbf{e}_i + \lambda L_{11}(\mathbf{u}_0, \mathbf{u}_i) = \mathbf{e}_i \quad (10)$$

$$\boldsymbol{\sigma}_i = H(\boldsymbol{\varepsilon}_i) = H(\mathbf{e}_i) \quad (11)$$

The variational strain becomes

$$\delta \boldsymbol{\varepsilon} = \delta \mathbf{e} + \xi_i L_{11}(\mathbf{u}_i, \delta \mathbf{u}) \quad (12)$$

By substituting (10) and (12) in the equilibrium equation (3) and taking into account the linear solution (6) the buckling is obtained by letting $\xi_i \rightarrow 0$

$$\lambda_i \boldsymbol{\sigma}_0 \cdot L_{11}(\mathbf{u}_i, \delta \mathbf{u}) + \boldsymbol{\sigma}_i \cdot \delta \mathbf{e} = 0 \quad (13)$$

The solution of the problem 13 yields the critical loads λ_i and the buckling modes \mathbf{u}_i . The buckling modes meet the following orthogonality condition:

$$\boldsymbol{\sigma}_0 \cdot L_{11}(\mathbf{u}_i, \mathbf{u}_j) = \delta_{ij} \quad (14)$$

Many relevant applications are characterized by closely-spaced buckling loads. This situation often lead to modal interaction that can remarkably affect the load carrying capacity of a certain structure. Moreover, different imperfection patterns can trigger different post-buckling paths. The asymptotic analysis is well suited to handle such cases with a highly reduced computational cost. The first step is to retain a certain number of modes M that are believed to interact. The post-buckling solution is then expanded as:

$$\mathbf{u} = \lambda \mathbf{u}_0 + \xi_i \mathbf{u}_i + \xi_i \xi_j \mathbf{u}_{ij} + \dots \quad (15)$$

where \mathbf{u}_{ij} can be considered as second order displacement fields that take into account the interaction of buckling modes \mathbf{u}_i and \mathbf{u}_j . The strain and the stresses are then expanded accordingly

$$\boldsymbol{\varepsilon} = \lambda \boldsymbol{\varepsilon}_0 + \xi_i \boldsymbol{\varepsilon}_i + \xi_i \xi_j \boldsymbol{\varepsilon}_{ij} + \dots \quad (16)$$

$$\boldsymbol{\sigma} = \lambda \boldsymbol{\sigma}_0 + \xi_i \boldsymbol{\sigma}_i + \xi_i \xi_j \boldsymbol{\sigma}_{ij} + \dots \quad (17)$$

where the second order strains and stresses are defined as follows

$$\boldsymbol{\varepsilon}_{ij} = L_1(\mathbf{u}_{ij}) + \frac{1}{2} L_{11}(\mathbf{u}_i, \mathbf{u}_j)$$

$$\boldsymbol{\sigma}_{ij} = H(\boldsymbol{\varepsilon}_{ij})$$

The correction fields \mathbf{u}_{ij} are the solution of the variational problem

$$\lambda \boldsymbol{\sigma}_0 \cdot L_{11}(\mathbf{u}_{ij}, \delta \mathbf{u}) + \boldsymbol{\sigma}_{ij} \cdot \delta \mathbf{e} = -\frac{1}{2} [\boldsymbol{\sigma}_i \cdot L_{11}(\mathbf{u}_j, \delta \mathbf{u}) + \boldsymbol{\sigma}_j \cdot L_{11}(\mathbf{u}_i, \delta \mathbf{u})] \quad (18)$$

Where λ is usually chosen as the minimum value of the buckling loads associated to the retained buckling modes. For consistency reasons, the second order correction fields \mathbf{u}_{ij} are required to be orthogonal to all buckling modes

$$\boldsymbol{\sigma}_0 \cdot L_{11}(\mathbf{u}_k, \mathbf{u}_{ij}) = 0, \quad (i, j, k) = [1, M] \quad (19)$$

By substituting the displacement expansion (15) into the equilibrium equation (3), after some manipulations the following system of reduced M nonlinear algebraic equilibrium equation is found

$$\xi_I \left(1 - \frac{\lambda}{\lambda_I} \right) + \xi_i \xi_j a_{ijI} + \xi_i \xi_j \xi_k b_{ijkI} = \frac{\lambda}{\lambda_I} \bar{\xi}_I \quad (20)$$

where $I = 1, 2, \dots, M$ and a general imperfection pattern $\bar{\mathbf{u}}$ is reproduced by a linear combination of the relevant M buckling modes included in the reduction basis, namely

$$\bar{\mathbf{u}} = \bar{\xi}_i \mathbf{u}_i \quad (21)$$

The system of equations (20) can be solved with a standard path-following technique. The formulas for the post-buckling coefficients a_{ijI}

and b_{ijkl} are written below. The first order coefficients a_{ijl} depend only on the pre-buckling solution \mathbf{u}_0 and the buckling modes \mathbf{u}_i . The calculation of the second order coefficients b_{ijkl} requires also the correction fields \mathbf{u}_{ij} .

$$a_{ijl} = \frac{\boldsymbol{\sigma}_I \cdot L_{11}(\mathbf{u}_i, \mathbf{u}_j) + 2\boldsymbol{\sigma}_i \cdot L_{11}(\mathbf{u}_j, \mathbf{u}_I)}{\boldsymbol{\sigma}_I \cdot \boldsymbol{\varepsilon}_I} \quad (22)$$

$$b_{ijkl} = [\boldsymbol{\sigma}_{Ii} \cdot L_{11}(\mathbf{u}_j, \mathbf{u}_k) + \boldsymbol{\sigma}_{ij} \cdot L_{11}(\mathbf{u}_k, \mathbf{u}_I) + \boldsymbol{\sigma}_I \cdot L_{11}(\mathbf{u}_i, \mathbf{u}_{jk}) + \boldsymbol{\sigma}_i \cdot L_{11}(\mathbf{u}_I, \mathbf{u}_{jk}) + 2\boldsymbol{\sigma}_i \cdot L_{11}(\mathbf{u}_j, \mathbf{u}_{kI})] / \boldsymbol{\sigma}_I \cdot \boldsymbol{\varepsilon}_I \quad (23)$$

3 Kinematic model

The nonlinear kinematic model considered in this study is the so-called *simplified Lagrangian* as proposed by [8]. This kinematic model neglects the quadratic stretch terms $u_{,x}^2$ and $v_{,y}^2$ that lead to erroneous calculations of post-buckling coefficients if the structure is iso-statically constrained. The strain-displacement function writes as follows

$$\begin{aligned} \varepsilon_x &= u_{,x} + \frac{1}{2}(v_{,x}^2 + w_{,x}^2) \\ \varepsilon_y &= v_{,y} + \frac{1}{2}(u_{,y}^2 + w_{,y}^2) \\ \gamma_{xy} &= u_{,y} + v_{,x} + w_{,x}w_{,y} \\ \chi_x &= w_{,xx} \\ \chi_y &= w_{,yy} \\ \chi_{xy} &= w_{,xy} \end{aligned} \quad (24)$$

The interested reader should refer to [8] for more details.

4 Finite Element implementation

Previous attempts in the implementation of Koiter's method in a finite element framework have highlighted the poor convergence of the post-buckling curvature coefficients b_{ijkl} when using

compatible finite elements. The problem is due to the different interpolation degrees of in-plane and out-of-plane displacements. Instead of adding extra nodes for the calculation of b_{ijkl} as in [11] or additional displacement fields as in [7] or using higher order *ad hoc* elements as in [9], we propose here a simple approach. The locking can be removed by averaging the in-plane strains thus leading to average quantities on the strain tensor. We chose for this study a 3 nodes triangular flat shell element with 6 degrees of freedom per node. The linear contribution is provided by the element generated by the template proposed by Felippa [5]. The drilling degree of freedom is consistently introduced without recurring to any artificial stiffness. In our particular case, the parameters for the template generate the element proposed by Allman, [1].

The kinematic model (24) can be written in finite element notation as

$$\boldsymbol{\varepsilon} = \begin{bmatrix} \varepsilon_x \\ \varepsilon_y \\ \gamma_{xy} \\ \chi_x \\ \chi_y \\ \chi_{xy} \end{bmatrix} = \left[\mathbf{B}_1 + \frac{1}{2}\mathbf{B}_2(\mathbf{u}_e) \right] \mathbf{u}_e \quad (25)$$

where \mathbf{u}_e is the element displacement vector, \mathbf{B}_1 is equivalent to the $L_1(\mathbf{u})$ operator of the general continuum formulation, and $\mathbf{B}_2(\mathbf{u}_e)$, equivalent to $L_2(\mathbf{u})$, is formulated as

$$\mathbf{B}_2 = [\mathbf{u}_e^T \mathbf{K}_{xx} \quad \mathbf{u}_e^T \mathbf{K}_{yy} \quad \mathbf{u}_e^T \mathbf{K}_{xy} \quad \mathbf{0} \quad \mathbf{0} \quad \mathbf{0}]^T \quad (26)$$

The matrices \mathbf{K}_{xx} , \mathbf{K}_{yy} and \mathbf{K}_{xy} contains the nonlinear terms of the kinematic model. These matrices are formed in a simple way. The shape functions for the displacements in the quadratic terms of the kinematic model are assumed as linear. This leads directly to constant strain components. The numerical results presented in the next section show that this simple approach yields fairly good results. The implementation advantages are remarkable. An already existing linear finite element has been used for the linear con-

tribution and the nonlinear terms can actually be based on a different formulation.

The whole analysis procedure can be translated in standard FE notation. The linear solution 6 is written as:

$$\mathbf{K}_0 \mathbf{u}_0 = \mathbf{F}_0 \quad (27)$$

where \mathbf{K}_0 is the material stiffness matrix and \mathbf{F}_0 is the vector of external forces. The buckling eigenvalue problem 13 is written as

$$[\mathbf{K}_0 - \lambda \mathbf{K}_G] \mathbf{u}_i = \mathbf{0} \quad (28)$$

where \mathbf{K}_G is the geometrical stiffness matrix. The linear problem for the second order fields \mathbf{u}_{ij} is written as

$$[\mathbf{K}_0 - \lambda \mathbf{K}_G] \mathbf{u}_{ij} = \mathbf{g}(\mathbf{u}_i, \mathbf{u}_j) \quad (29)$$

with the orthogonality condition

$$\mathbf{u}_k^T \mathbf{K}_G \mathbf{u}_{ij} = 0 \quad (30)$$

The forcing term $\mathbf{g}(\mathbf{u}_i, \mathbf{u}_j)$ is formed through an assembly operation of contribution calculated at element level. For an element, this writes:

$$\begin{aligned} \mathbf{g}_e(\mathbf{u}_{e_i}, \mathbf{u}_{e_j}) = & -\frac{1}{2} \mathbf{A} [\mathbf{u}_{e_i}^T \mathbf{B}_1^T \mathbf{C}_m \mathbf{B}_2(\mathbf{u}_{e_j}) + \\ & \mathbf{u}_{e_j}^T \mathbf{B}_1^T \mathbf{C}_m \mathbf{B}_2(\mathbf{u}_{e_i}) + \\ & \mathbf{u}_{e_i}^T \mathbf{B}_2(\mathbf{u}_{e_j}) \mathbf{C}_m \mathbf{B}_1]^T \end{aligned} \quad (31)$$

where \mathbf{A} is the element area, \mathbf{u}_{e_i} and \mathbf{u}_{e_j} are the element components of buckling modes \mathbf{u}_i and \mathbf{u}_j respectively, and \mathbf{C}_m is the membrane material tensor.

5 Numerical examples

5.1 Rectangular plates

The proposed formulation is tested on rectangular plates of different aspect ratios loaded in compression and shear. Different boundary conditions are considered. These test were presented by Lanzo *et al.* in [9] where High Continuity (HC) flat elements were used. The different configurations are sketched in Figure 1 and 2. The numerical results are reported in Table 1 and 2. The convergence of the results is good in all the considered cases.

5.2 Cylindrical shell under external pressure

A cylindrical shell is considered here. The bottom edge is restrained against translational displacements while the top edge is free to move along the longitudinal axis of the shell. The radial displacement of the top edge is restrained as well. The shell is loaded with a uniform external pressure. Only 1/8 of the structure is modeled, i.e. three planes of symmetry have been considered: one normal to the longitudinal axis of the shell and the other two normal to each other cutting the shell in the longitudinal direction. In order to show the convergence properties of the proposed technique, one buckling mode with 16 half-waves in the circumferential direction is considered. Table 3 shows the results. The grid size reported in the first column refers to the number of nodes in the longitudinal on the circumferential direction of the reduced respectively. The present results are compared with results obtained by a semi-analytical approach using assumed mode shapes [2] and Donnell's shell theory. The slight discrepancy of the buckling load might be due to the approximation of the Donnell's theory as compared to full finite element analysis. The b coefficient is calculated assuming the normalization condition 14 for the buckling mode. The results obtained according to [2] normalized the buckling mode for a maximum radial displacement equal to one thickness of the shell. The last two columns of Table 3 report the calculated scale factor and the scaled b coefficient to allow for a direct comparison. Figure 3 shows the considered buckling mode \mathbf{u}_1 and the corresponding second order field \mathbf{u}_{11} . It can be noticed that the buckling mode does not contain any axisymmetric component. The second order field results in twice the number of circumferential half-waves of the buckling mode. In addition, an axisymmetric contraction is also present. These shapes coincide with those predicted by the semi-analytical approach with assumed buckling mode shapes [2]. This constitutes a further confirmation of the correctness of the approach.

Case	Mesh	$\lambda_1 \cdot \left(\frac{\pi^2}{b^2} \frac{Eh^3}{12(1-\nu^2)} \right)^{-1}$	Lanzo et al.[9]	b	Lanzo et al.[9]
Test A1 a/b=1	10 x 10	4.0388362	4.00263 (25x25)	0.191883214	0.18244 (25x25)
	15 x 15	4.017149563		0.191723948	
	20 x 20	4.009624355		0.18563007	
	25 x 25	4.006153333		0.186080096	
Test A2 a/b=1	10 x 10	8.04340086	7.71346 (33x33)	0.223001109	0.195755 (33x33)
	15 x 15	7.843668665		0.205346549	
	20 x 20	7.776080091		0.198469215	
	25 x 25	7.745257369		0.199548785	
Test A3 a/b=2	20 x 10	1.385799166	1.38808 (33x17)	0.012169656	0.008805 (33x17)
	30 x 15	1.386037362		0.010546446	
	40 x 20	1.386110606		0.009797109	
Test A4 a/b=2	20 x 10	4.946837992	4.854951 (49x21)	0.263218974	0.260825 (49x21)
	30 x 15	4.890945913		0.265622193	
	40 x 20	4.871677155		0.262086004	

Table 1 Rectangular plates: compression results

Case	Mesh	$\lambda_1 \cdot \left(\frac{\pi^2}{b^2} \frac{Eh^3}{12(1-\nu^2)} \right)^{-1}$	Lanzo et al.[9]	b	Lanzo et al.[9]
Test C1 a/b=1	10 x 10	9.416258309	9.35185 (25x25)	0.116091233	0.114525 (25x25)
	15 x 15	9.377094299		0.11697097	
	20 x 20	9.351758761		0.115212276	
	25 x 25	9.342275615		0.115645483	
a/b=2	10 x 20	6.682043757	6.56822 (23 x 45)	0.073600212	0.071705 (23 x 45)
	15 x 30	6.594218494		0.073809291	
	20 x 40	6.580867051		0.072355707	
a/b=3	10 x 30	5.943129417	5.8846 (15x45)	0.083668132	0.07992 (33x17)
	15 x 45	5.886262178		0.081203308	
Test C2 a/b=1	10 x 10	15.48723676	14.7822 (25x25)	0.110508211	0.116855 (25x25)
	15 x 15	15.00922184		0.116438822	
	20 x 20	14.84667709		0.11531944	
	25 x 25	14.77238119		0.116812549	
a/b=2	10 x 20	10.67048378	10.34334 (23 x 45)	0.13772903	0.13282 (23 x 45)
	15 x 30	10.43363845		0.131617299	
	20 x 40	10.35192712		0.132752763	
a/b=3	10 x 30	9.896498384	9.74613 (15x45)	0.086245608	0.086505 (15x45)
	15 x 45	9.694008245		0.087441679	

Table 2 Rectangular plates: shear results

Mesh	λ	b	α	$\frac{b}{\alpha^2}$
15 x 95	1.373881273	-4.752465986	5.347208965	-0.166212891
20 x 126	1.368859542	-4.944148739	5.336236754	-0.173628634
25 x 158	1.366456287	-5.040884291	5.338352961	-0.176885469
30 x 189	1.365180404	-5.093376464	5.343454282	-0.178386334
35 x 220	1.364402866	-5.125336846	5.370763223	-0.17768485
40 x 252	1.363877522	-5.144431862	5.409906622	-0.175775314
45 x 283	1.36352264	-5.158591033	5.393886537	-0.177307655
50 x 315	1.3632541	-5.17027873	5.362566608	-0.179791252
From [2]	1.3448			-0.180887

Table 3 Cylindrical shell results

5.3 T-section beam

The last example considers a T-section beam that can be considered as an assembly of flat plates. The material and geometric properties and the boundary conditions are shown in Figure 4. This example is reported in literature [8] as a structure that exhibits an unstable post-buckling behavior caused by the interaction of the first two buckling modes. Figure 7 shows the convergence of the components of the b tensor. The grid size reported on the horizontal axis refers to the number of nodes in half of the horizontal flange. Figure 8 shows a comparison between a full nonlinear analysis with the commercial finite element program ABAQUS and a Koiter's analysis with the presented approach. The lateral displacement of the point of application of the load is monitored. The ABAQUS model shares the same mesh fineness as the finest model considered for the Koiter's analysis ($n=10$). The S4R shell element is used. The geometric imperfection is in the shape of the first buckling mode as to impose a stress-free maximum displacement of 0.01 mm in the vertical direction. The limit load is quite well captured by the Koiter's analysis in spite of all the simplifications implied in the asymptotic method.

6 Conclusions

A new finite element implementation of Koiter's analysis has been presented. We showed that good convergence of the post-buckling coefficients can be obtained without relying upon *ad*

hoc techniques or special finite element formulations. A simple and effective 3 nodes triangular linear shell element has been enriched to model quadratic kinematic terms. These terms were modeled by using simple linear shape functions leading to constant strains thus avoiding locking. Numerical experiments showed good comparisons with results available in the literature.

References

- [1] D. J. Allman. A basic facet finite element for the analysis of general shells. *International Journal for Numerical Methods in Engineering*, 37:19–35, 1994.
- [2] J. Arbocz and J.M.A.M. Hol. Koiter's stability theory in a computer-aided engineering (cae) environment. *International Journal of Solids Structures*, 26:945–975, 1990.
- [3] B. Budiansky. Dynamic buckling of elastic structures: criteria and estimates. In *Dynamic Stability of Structures*. Pergamon Press, 1965. Proceedings of International Conference, Northwestern University, Evanston, Illinois.
- [4] J. W. Hutchinson E. Byskov. Mode interaction in axially stiffened cylindrical shells. *AIAA Journal*, 15:941–948, 1977.
- [5] C.A. Felippa and C. Militello. Construction of optimal 3-node plate bending triangles by templates. *Computational Mechanics*, 24:1–13, 1999.
- [6] A. D. Lanzo G. Salerno. A nonlinear beam finite element for the post-buckling analysis of plane frames by koiter's perturbation approach. *Com-*

- puter Methods in Applied Mechanics and Engineering*, 146:325–249, 1997.
- [7] E. Byskov J. F. Olesen. Accurate determination of asymptotic postbuckling stresses by the finite element method. *Computer & Structures*, 15:157–163, 1982.
- [8] A.D. Lanzo and G. Garcea. Koiter’s analysis of thin-walled structures by a finite element approach. *International Journal for Numerical Methods in Engineering*, 39:3007–3031, 1996.
- [9] A.D. Lanzo, G. Garcea, and R. Casciaro. Asymptotic post-buckling analysis of rectangular plates by hc finite elements. *International Journal for Numerical Methods in Engineering*, 38:2325–2345, 1995.
- [10] C. M. Menken, G. M. A. Schreppers, W. J. Groot, and R. Petterson. Analyzing buckling mode interactions in elastic structures using an asymptotic approach; theory and experiment. *Computer & Structures*, 64:473–480, 1997.
- [11] L. Damkilde P. N. Poulsen. Direct determination of asymptotic structural postbuckling behavior by the finite element method. *International Journal for Numerical Methods in Engineering*, 42:685–702, 1998.
- [12] E. Riks, C. C. Rankin, and F. Brogan. On the solution of mode jumping phenomena in thin-walled structures. *Computer Methods in Applied Mechanics and Engineering*, 136:59–92, 1996.

KOITER'S POST-BUCKLING ANALYSIS OF GENERAL SHELL STRUCTURES USING THE FINITE ELEMENT METHOD

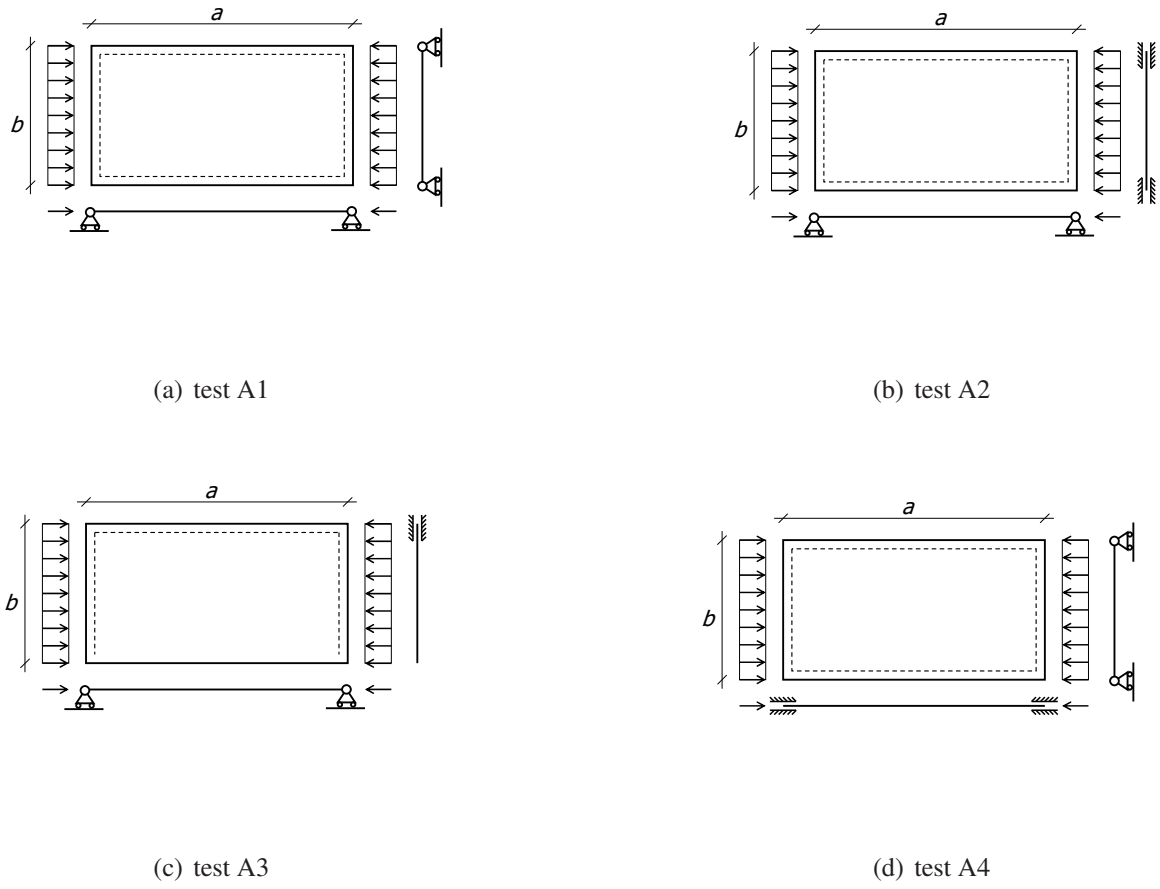


Fig. 1 Rectangular plates: compression case studies

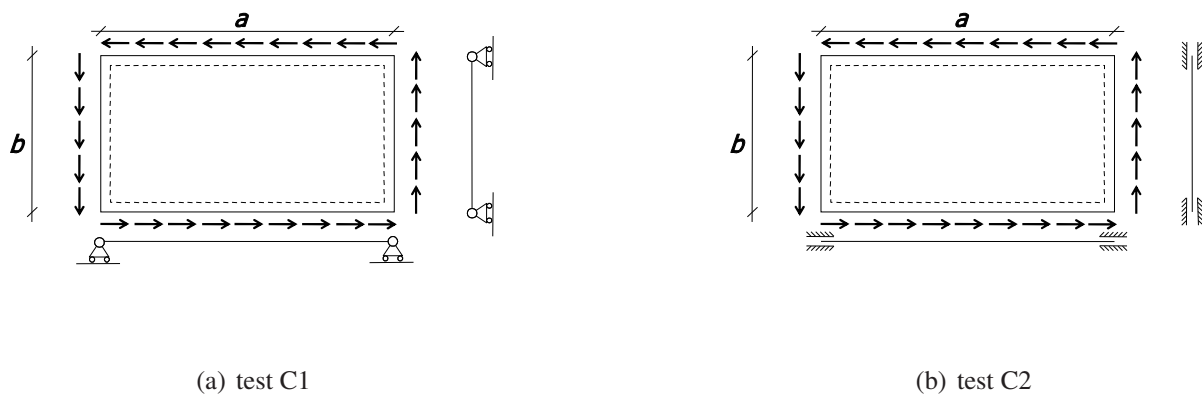


Fig. 2 Rectangular plates: shear case studies



Fig. 3 Cylindrical shell: buckling load and second order field

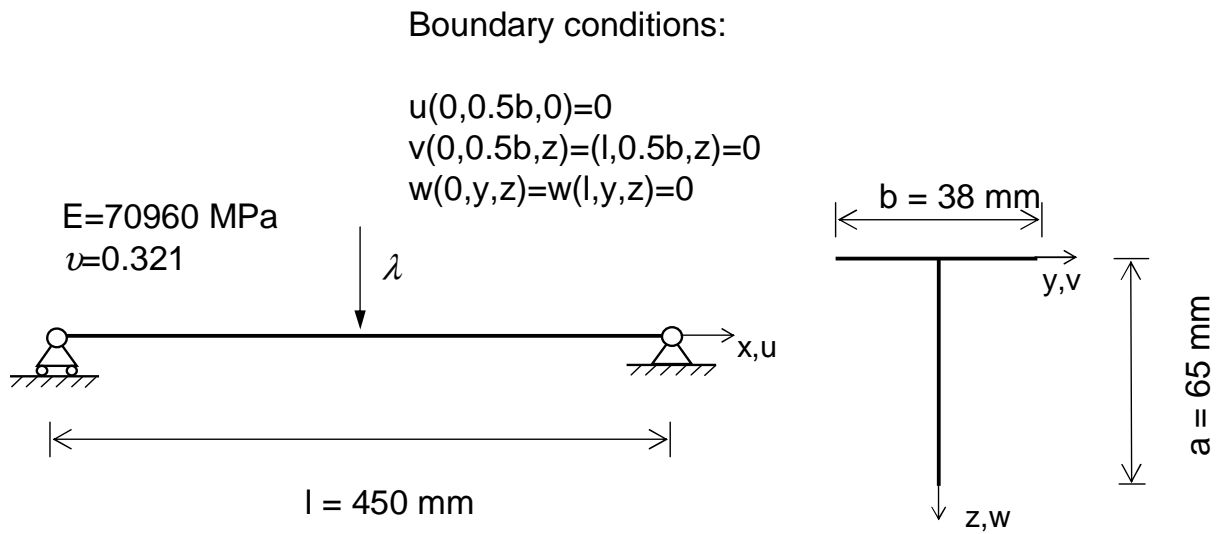


Fig. 4 T-section beam

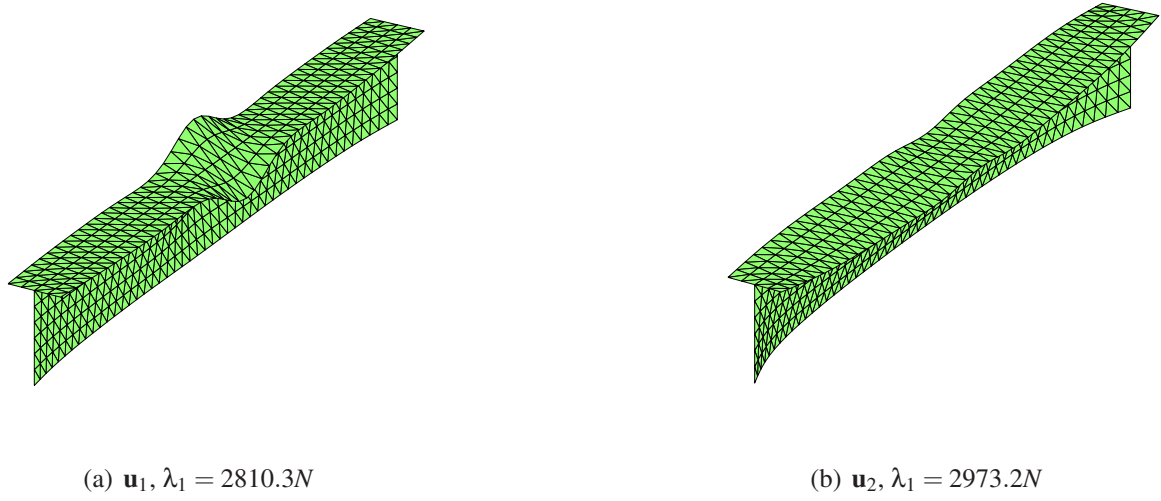


Fig. 5 T-section beam:buckling modes

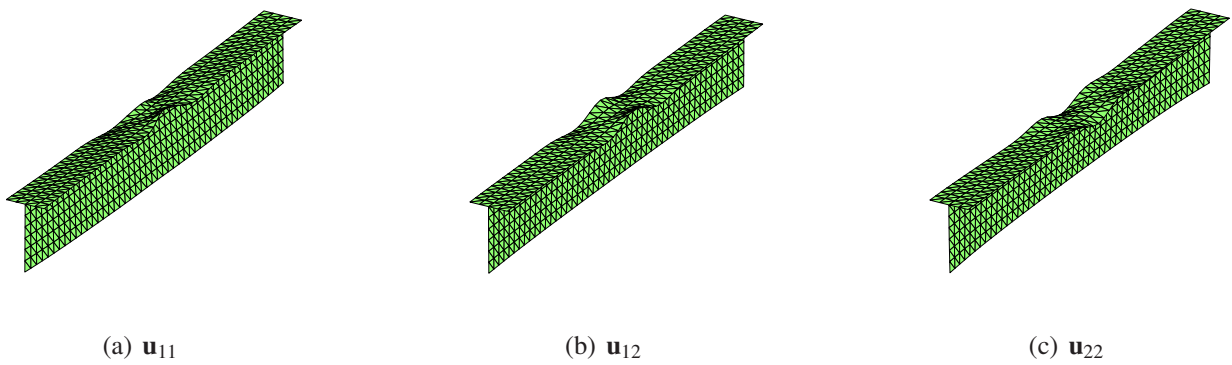


Fig. 6 T-section beam:second order fields

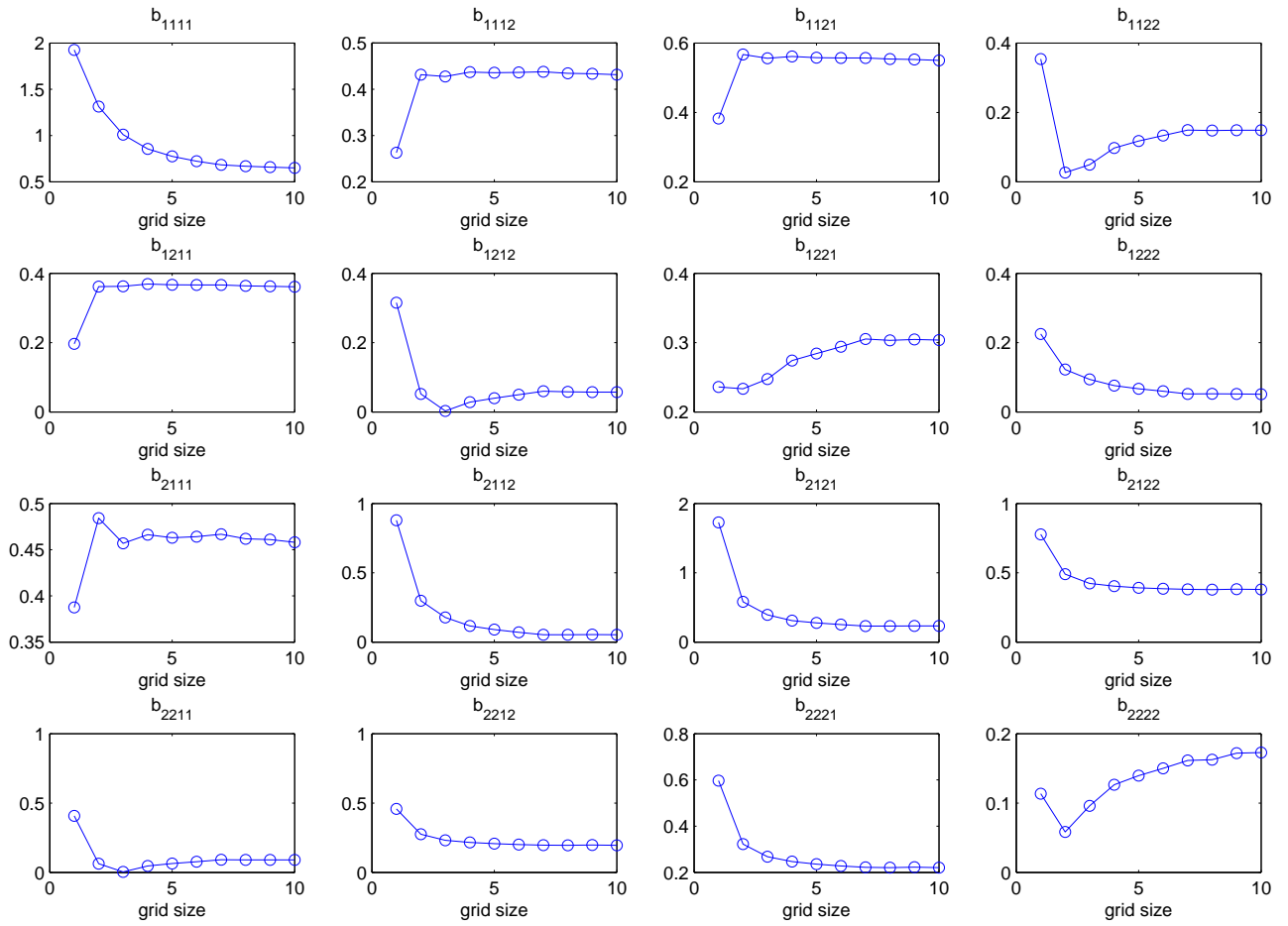


Fig. 7 T-section beam: convergence of b_{ijkl}

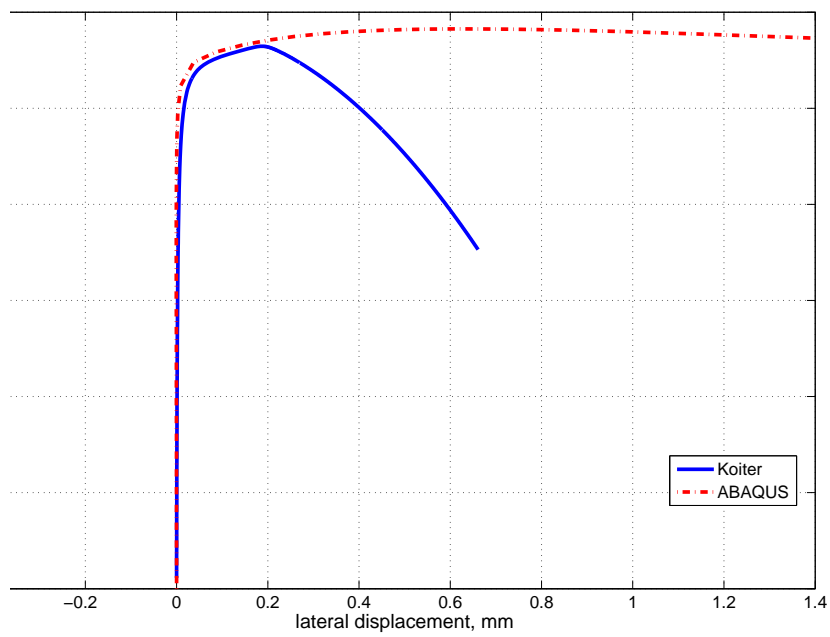


Fig. 8 T-section beam: comparison with ABAQUS full nonlinear analysis